

Quantum Circuit Transformation Based on Subgraph Isomorphism and Tabu Search^{*}

First Aaaaaauthor¹[0000-*ereer*1111-2222-3333], Second Author^{2,3}[1111-2222-3333-4444], and Third Author³[2222--3333-4444-5555]

¹ Princeton University, Princeton NJ 08544, USA

² Springer Heidelberg, Tiergartenstr. 17, 69121 Heidelberg, Germany

lncs@springer.com

<http://www.springer.com/gp/computer-science/lncs>

³ ABC Institute, Rupert-Karls-University Heidelberg, Heidelberg, Germany
{abc,lncs}@uni-heidelberg.de

Abstract. The goal of quantum circuit adjustment is to construct mappings from logical quantum circuits to physical ones in an acceptable amount of time, and in the meantime to introduce as few auxiliary gates as possible. We present an effective approach to constructing the mapping. It consists of two keys steps: one makes use of a combined subgraph isomorphism and complement (CSIC) to initialize a mapping, the other dynamically adjusts the mapping by using a Tabu search based adjustment (TSA). Our experiments show that, compared with the wghtgraph recently considered in the literature, CSIC can save 22.26% of auxiliary gates and reduce the depths of output circuits by 11.76% on average in the initialization of the mapping, and TSA has a better scalability than many state-of-the-art algorithms for adjusting mappings.

Keywords: Quantum circuit transformation · Subgraph isomorphism · Initial mapping · Tabu search

1 Introduction

The entanglement of a quantum system with its surrounding environment will lead to quantum decoherence. It is unrealistic to use quantum error correction in circuit mapping process, since there are only dozens of available qubits for quantum devices in the NISQ era [16]. It is necessary to transform circuits by adding auxiliary gates to satisfy both logical and physical constraints, since quantum algorithms do not consider any hardware connectivity constraints. Hence, quantum circuit transformation is an important part of quantum circuit compilation. We need a set of highly efficient and automatic mapping procedures and adjustment routines to perform circuit transformation. In this process noise may be introduced, which brings a huge challenge to circuit compilation because noise has a significant impact on the final circuit and may make the result meaningless.

^{*} Supported by organization x.

In the current work, we adjust the lifetime of qubits through parallelization, and use SubgraphMatching [20] to generate partial isomorphic subgraphs of logical circuits and physical circuits as part of the initial mapping. The advantage of the initial mapping result is that we use the appropriate subgraph isomorphism and the two-way connection of the logical circuit and the physical circuit to obtain a dense initial mapping, which avoids certain nodes from being mapped to remote locations. We use Tabu search [6] to generate circuits that can be executed on physical devices. Tabu search can avoid falling into local optimum and swapping the recently swapped qubits, thereby improve the parallelism of quantum gates. We add SWAP gates associated with the gates on the shortest path to the candidate set, which greatly reduces the search space and improves the search speed. Our heuristic function not only considers the current gates but also the constraints of the gates already considered.

We compare CSIC with the state-of-the-art initial mapping methods wght-graph [10] and optm [25]. On average, the auxiliary gates of the CSIC algorithm are reduced by 22.44% (resp. 27.02%), and the depths are reduced by 11.25% (resp. 14.12%). We compare TSA with wgtgraph [10] and SABRE [9]. On the one hand, TSA can deal with 159 circuits in a few minutes, while the other two adjustment algorithms are difficult to handle medium-sized or large circuits. On the other hand, the number of SWAP gates added by wgtgraph is 26.87% (resp. 24.89%) smaller than that of TSA on average. Among the 159 circuits that we also test with SABRE, only 29 can be successfully mapped within the five-minute limit.

The main contributions of this paper are as follows.

1. We propose to use the combined subgraph isomorphism algorithm to generate part of the initial mapping and then complete the mapping based on the connectivity between qubits.
2. We present a heuristic circuit adjustment algorithm based on Tabu search [6], which can handle large circuits in a shorter time at a lower cost, compared with existing precise search and heuristic algorithms.
3. We put forward a look-ahead heuristic function that considers both the current gates and the gates yet to be processed. It filters out SWAP gates that are beneficial to the current gates and also bring closer the gates to be processed.
4. We test 159 circuits, and the results show that the initial mapping generated by our method requires to insert fewer SWAP gates, and the adjustment algorithm can be extended to handle medium-sized and large circuits.

The rest of this paper is organized as follows. In Section 2 we discuss some related work. In Section 3 we recall some background of quantum computing and quantum information. In Section 4 we introduce the problem of quantum circuit transformation provide our solution by describing our algorithm in detail. The experimental results are reported in Section 5. The last section concludes the paper and discusses some future research.

2 Related work

Quantum technology has been applied in practice, but large quantum computers have not yet been built. Most of the contributions of quantum information to computer science are still in the theoretical stage. In 2017, IBM developed the first 5-qubit backend called IBM QX2, followed by the 16-qubit backend IBM QX3. The revised versions of them are called IBM QX4 and IBM QX5, respectively. IBM Q Experience provides the public with free quantum computer resources on the cloud and opens source the quantum computing software framework *Qiskit*⁴.

Users of these early quantum computers mainly rely on quantum circuits to implement quantum algorithms. They design logical circuits which then go through the step of circuit transformation in order to map logical qubits to physical ones before the logical circuits are executed in physical devices. A big challenge for quantum information is the problem of quantum decoherence. Due to the decoherence of qubits, quantum gates need to be applied in a coherent period as the time for a qubit to stay in a coherent state is very short. The longest coherence time of a superconducting quantum chip is still within 10us-100us.

There are several initial mapping methods. Paler [15] has showed that the initial mapping has an important influence on quantum circuit transformation. He proposed a heuristic method to find the initial mapping. Just by placing qubits in different positions from the default trivial placement in the actual circuit instances on the actual NISQ device, the time cost can be reduced by up to 10%. Li et al. [9] have proposed a novel reverse traversal technique, which determines the initial mapping by considering the entire circuit. Zhou et al. [23] have put forward an annealing algorithm to find an initial mapping, but it is unstable. In [10], Li et al. have considered the subgraph isomorphism algorithm wghtgraph to generate an initial mapping, which is the most recent result, so we will compare with it.

The goal of circuit adjustment algorithm is to minimize the number of auxiliary SWAP gates. There are currently five main methods for solving the quantum circuit adjustment problem.

- *Unitary matrix decomposition algorithm.* It is used in [8, 14] to rearrange the quantum circuit from the beginning while retaining the input circuit. It can be applied to a broad class of circuits consisting of generic gate sets, but the results are not as efficient as a compiler designed specifically for this task.
- *Converting into some existing problems.* This approach converts the quantum circuit transformation problem into some existing problems, such as AI planning [22, 3], Integer Linear Programming (ILP) [1], or Satisfiability Modulo Theories (SMT) [12]. Existing tools for those problems are then used to find acceptable results. The approach cannot take advantage of certain properties of quantum mapping, which is a drawback. Furthermore, as the time cost is usually long, it can only deal with small quantum circuits.

⁴ <https://www.qiskit.org/>

- *Exact methods.* Siraichi et al. [19] have proposed an exact method. It will iterate all possible mappings for all dependencies, so it is only suitable for simple quantum architecture and cannot be extended to complex quantum architectures.
- *Graph theory.* In [17], Shafaei et al. have used the minimum linear permutation solution in graph theory to model the problem of reducing the interaction distance. The idea is to first divide a given circuit into several subcircuits and apply the minimum linear permutation solution, respectively. Then we turn non-adjacent gates in the subcircuits into adjacent gates by adding auxiliary gates. Finally, we can use the minimum linear permutation solution to find an appropriate permutation and use bubble sort to calculate the number of necessary SWAP gates. In [7, 11], a two-step method is used to reduce the quantum circuit transformation to the graph problem to minimize the number of auxiliary gates, based on the graph coloring problem and the largest subgraph isomorphism problem.
- *Heuristic search.* Heuristic search uses an evaluation function to obtain an acceptable solution in exponential time. Zulehner et al. [25] have suggested to layer the circuits, then determine compatible mappings for each of these layers to add as few auxiliary gates as possible. Zhou et al. [23] have designed a heuristic search algorithm with a novel selection mechanism. Instead of choosing the operation with the lowest cost to apply, one can look forward one step and then choose the best continuous operation. In this way, the algorithm can effectively avoid local minimum. Moreover, a pruning mechanism is introduced to reduce the search space’s size and ensure that the program terminates in a reasonable amount of time.

Li et al. [9] have proposed a SWAP-based search algorithm SABRE. Compared with previous search algorithms based on exhaustive mapping, SABRE can adapt to large quantum circuits in the NISQ era. In [4], a routing algorithm called $t|ket\rangle$ ensures that any quantum circuit can be compiled into any architecture. The algorithm is divided into four stages: decomposing the input circuit into time steps, determining the initial mapping, routing across time steps, and finally cleaning up. The heuristics in $t|ket\rangle$ give the same or better results than other circuit transformation systems in terms of the depth and the total number of gates in the compiled circuit, with much shorter running time, and can handle larger circuits. In [21], a variation-aware qubit movement strategy is proposed. It takes advantage of the change in error rate and a change-aware quantum circuit transformation strategy by trying to select the route with the lowest probability of failure. This strategy uses the error rate of SWAPs to allocate logical qubits to physical qubits, thus avoiding paths with high error rates as much as possible.

Among the existing methods above, wghtgraph [10] and optm [25] are probably the most effective initial mapping ones. As to circuit adjustment algorithms, wgtgraph [10] and SABRE [9] represent the state of the art. Therefore, we choose to compare our solution with them in Section 5.

3 Preliminary

In this section we introduce some notions and notations of quantum computing and quantum information.

Classical information is stored in bits, while quantum information is stored in qubits. Besides two basic states $|0\rangle$ and $|1\rangle$, a qubit can be in any linear superposition state like $|\phi\rangle = a|0\rangle + b|1\rangle$, where $a, b \in \mathbb{C}$ satisfy the condition $|a|^2 + |b|^2 = 1$. The intuition is that $|\phi\rangle$ is in the state $|0\rangle$ with the probability $|a|^2$ or in the state $|1\rangle$ with the probability $|b|^2$. We use letters \mathbf{q} and q in different fonts to represent physical qubits and logical qubits.

By applying quantum gates to qubits, we can change their states. For example, the Hadamard gate (H gate) can be applied on a single qubit, while the CNOT gate can be applied on two qubits. Their representations in terms of gate symbols and their semantics in terms of matrices are shown in Fig. 1.

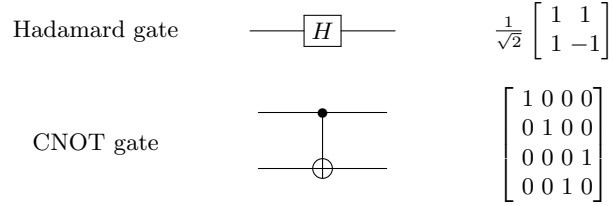


Fig. 1. The symbols of two quantum gates and their matrices

A quantum logical circuit consists of quantum gates interconnected by quantum wires [5]; see Fig. 2 for an example. A quantum wire is a mechanism for moving quantum data from one location to another. Each line represents a qubit, and the gates on the lines act on the corresponding qubits. The execution order of a quantum logical circuit is from left to right. The width of a circuit refers to the number of qubits in the circuit. The depth of a circuit refers to the number of layers executing in parallel. For example, the depth of the circuit in Fig. 2 is 6, and the width is 5. In this paper, a circuit with a depth less than 100 is called a small circuit, a circuit with a depth greater than 1000 is called a large circuit, and the rest are medium-sized circuits. It is unnecessary to consider quantum gates acting on single qubits in circuit adjustments, since the single qubits are *local* [18].

In the current work, we mainly consider the physical circuits of the IBM Q series. Let $\mathcal{AG}_{\mathcal{P}} = (V_{\mathcal{P}}, E_{\mathcal{P}})$ denote the architecture graph of a physical circuit, where $V_{\mathcal{P}}$ denotes the set of physical qubits and $E_{\mathcal{P}}$ denotes the set of edges that connect CNOT gates. In Fig. 3, diagrams (a) and (b) are the physical architecture graphs of the 5-qubit IBM QX2 and IBM QX4, respectively; diagrams (c) and (d) are the physical architecture graphs of the 16-qubit IBM QX3 and IBM

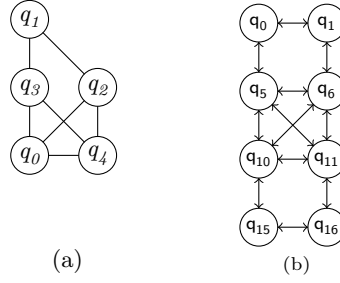


Fig. 4. (a) The architecture graph of original circuit in Fig. 2. (b) The partial architecture graph of IBM Q20.

Example 1. Fig. 4 (a) is the logical structure of Fig. 2. Fig. 4 (b) is the partial architecture graph of IBM Q20. An initial mapping is

$$\tau = \{q_0 \rightarrow q_{10}, q_1 \rightarrow q_0, q_2 \rightarrow q_6, q_3 \rightarrow q_5, q_4 \rightarrow q_{11}\}.$$

The 2-qubit gate $g_0 = \langle q_2, q_1 \rangle$ is not executable, since the edge $\langle \tau(q_2), \tau(q_1) \rangle = \langle q_6, q_0 \rangle$ does not exist in \mathcal{AG}_P . But $g_3 = \langle q_1, q_3 \rangle$ is executable, since the edge $\langle \tau(q_1), \tau(q_3) \rangle = \langle q_0, q_5 \rangle$ exists in \mathcal{AG}_P .

4 Quantum Circuit Transformation

A common assumption for circuit transformation is that we are given a circuit that has only single quantum gates and CNOT gates [2, 13]. We add auxiliary gates to move two non-adjacent qubits to adjacent positions or change the direction of a CNOT gate. Adding more gates increases the risk of introducing more noise. Therefore, we hope to find a circuit transformation algorithm that, when given an input circuit, can produce an output circuit with a minimal number of auxiliary gates and a small circuit depth in an acceptable amount of time.

Roughly speaking, quantum circuit transformation includes the following three steps.

1. *Preprocessing.* This step includes extracting the logical architecture graph of the circuit, adjusting the life cycle of qubits as in [24], and calculating the shortest paths of the physical circuit.
2. *Isomorphism and completion.* This step uses the subgraph isomorphism algorithm to find part of the initial mapping [20]. Then we perform a mapping completion to include the remaining nodes that do not satisfy all isomorphism requirements, according to the connectivity between the unmapped node and the mapped nodes.
3. *Adjustment.* After the second step, some logically adjacent nodes may be mapped to physically non-adjacent nodes, thus quantum gates applied on

them cannot be executable on physical devices. It is necessary to adjust the quantum circuits by adding auxiliary gates to swap qubits. We use Tabu search for the adjustment so as to generate circuits that can be physically executed.

Note that isomorphism and adjustment are both NP-complete [19]. So we make use of some heuristics. Below we give a detailed account of each of the steps.

4.1 Preprocessing

In the preprocessing step, we adjust the input circuit described by an openQASM program to shorten the life cycle of qubits. Then we use a Breadth-First Search (BFS) to calculate the shortest distance between each pair of nodes on the architecture graph.

We use a layered method to analyze the life cycle of qubits and pack the gates that can be executed in parallel into a *bundle*, forming a layered bundle format [24]. A conversion method is designed to use the layered bundle format to determine which gates can be moved so the qubits related to these gates can reduce their life cycles, and the execution time of quantum programs can also be reduced.

Quantum gates acting on different qubits can be executed in parallel. Therefore, we classify the gates that can be executed in parallel into one layer, otherwise we add a new layer. The notation $L(LC) = \{\mathcal{L}_0, \mathcal{L}_1, \dots, \mathcal{L}_n\}$ represents the layered circuit, where \mathcal{L}_i ($0 \leq i \leq n$) stands for a quantum gate set that can be executed in parallel. The quantum gate set separated by the dotted line in Fig. 2 are the following $\mathcal{L}_0 = \{g_0, g_1\}$, $\mathcal{L}_1 = \{g_2\}$, $\mathcal{L}_2 = \{g_3, g_4\}$, $\mathcal{L}_3 = \{g_5, g_6\}$, $\mathcal{L}_4 = \{g_7\}$, $\mathcal{L}_5 = \{g_8\}$.

At the same time of circuit layering, we generate a logical circuit architecture graph $\mathcal{AG}_L = (V_L, E_L)$, which is an undirected graph with V_L being the set of vertices, and E_L the set of undirected edges that represent the connectivity between qubits related by CNOT gates. Given a physical architecture graph and assume the distance of each edge is 1, we can use Floyd-Warshall algorithm to calculate the shortest distance matrix $dist[i][j]$, which represents the shortest distance from q_i to q_j .

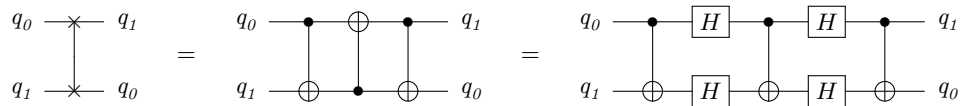


Fig. 5. Implenting a SWAP gate by using CNOT gates and H gates

For IBM QX2, QX3, QX4, and QX5, the control of one qubit to a neighbour is unilateral. In this case, a SWAP gate can be implemented by using three CNOT gates and four H gates, as shown in Fig. 5. The four H gates are needed

to change the direction of the middle CNOT gate. Consider a CNOT gate $g = \langle q_i, q_j \rangle$. If q_i and q_j are mapped to q_m and q_n , respectively, then the cost of executing g under the shortest path is $cost_{cnot}(q_i, q_j) = 7 \times (dist[m][n] - 1)$. For IBM Q20, where the control between two adjacent qubits are bilateral, a SWAP gate can be implemented by using three CNOT gates. Thus the cost is $cost_{cnot}(q_i, q_j) = 3 \times (dist[m][n] - 1)$. The time complexity is $O(N^3)$.

Example 2. Take the QX5 (cf. Fig. 3 (d)) structure as an example. Suppose there is a CNOT gate $g = \langle q_1, q_2 \rangle$, with q_1 mapped to q_1 and q_2 mapped to q_{14} . The shortest distance between them is $dist[1][14] = 3$. There are 3 shortest paths to move q_1 to an adjacent position of q_{14} : $\pi_0 = q_1 \rightarrow q_2 \rightarrow q_3 \rightarrow q_{14}$, $\pi_1 = q_1 \rightarrow q_2 \rightarrow q_{15} \rightarrow q_{14}$, $\pi_2 = q_1 \rightarrow q_0 \rightarrow q_{15} \rightarrow q_{14}$. Their costs are given by $cost_{\pi_0} = 18$, $cost_{\pi_1} = 14$, and $cost_{\pi_2} = 14$, respectively.

4.2 Isomorphism and Completion

In general, in a physical architecture graph, it is almost impossible to find a subgraph that exactly matches all the nodes in a logical architecture graph. We regard the mapping with the largest number of matching nodes as the partial mapping. SubgraphMatching compares various compositions of several state-of-the-art subgraph isomorphism algorithms. It shows that the best performance can be achieved by using filters and the sorting ideas of the GraphQL algorithm to process candidate nodes, and the local candidates calculation method LFTJ based on set-intersection to enumerate the results. Since SubgraphMatching cannot handle disconnected graphs, we artificially create connected graphs by connecting isolated nodes to the nodes with the largest degree in the logical architecture graph.

The input of Algorithm 1 is a target graph (\mathcal{AG}_P), a query graph (\mathcal{AG}_L), and the partial mapping set T . First, we initialize an empty queue Q . Then we traverse τ and add the unmapped nodes to the queue Q . For the unmapped nodes, we try to map them to the vicinity of the mapped nodes in \mathcal{AG}_P . If a node q is not mapped to any physical node, we need to perform such kind of mapping completion. Finally, we generate a dense mapping, which can reduce the added auxiliary gates. In principle, we could try to match the remaining unmapped nodes randomly, but it may lead to a mapping with a node far away from other nodes. If an unmapped node has an edge adjacent to a matched node in the query graph, it will be matched to one of the adjacent nodes first. In this way, we can obtain all initial candidate mappings.

Example 3. Following the previous example, we first use the CSIC algorithm for the logical architecture graph given in Fig. 4 (a) and the physical architecture graph given in Fig. 3 (e) to obtain the partial mapping set $T = \{\tau_0, \tau_1, \dots, \tau_n\}$. We take one of the partial mappings as an example.

$$\tau_0 = \{q_0 \rightarrow q_{10}, q_1 \rightarrow -1, q_2 \rightarrow q_6, q_3 \rightarrow q_5, q_4 \rightarrow q_{11}\}.$$

Here $q_1 \rightarrow -1$ means that q_1 is not mapped to any physical node, so we need to perform a mapping completion. In this example, the maximum number of

Algorithm 1: Complementary mapping algorithm based on connectivity between qubits

Input: $\mathcal{AG}_{\mathcal{L}}$: The architecture of logical circuit
 $\mathcal{AG}_{\mathcal{P}}$: The architecture of physical circuit
 T : A partial mapping set obtained by SubgraphMatching
Output: *result*: A collection of mapping relations between $\mathcal{AG}_{\mathcal{L}}$ and $\mathcal{AG}_{\mathcal{P}}$

```

1 Initialize result =  $\emptyset$  ;
2  $l \leftarrow \max_{\tau \in T} \tau.length$ ;
3 for  $\tau \in T$  do
4   if  $l = \tau.length$  then
5     result.add( $\tau$ );
6      $Q \leftarrow$  an empty unmapped node queue
7      $i \leftarrow 1$ ;
8     while  $i \leq \tau.length$  do
9        $Q.push(\{i, i \leq \tau.length\})$ 
10       $i \leftarrow i + 1$ ;
11     while  $Q$  is not empty do
12        $q \leftarrow Q.poll()$ ;
13        $targetAdj \leftarrow \mathcal{AG}_{\mathcal{P}}.adjacencyMatrix()$ ;
14        $queryAdj \leftarrow \mathcal{AG}_{\mathcal{L}}.adjacencyMatrix()$ ;
15        $cans \leftarrow$  an empty candidate node list sorted by degree
16        $cans \cup \{q_m, q_m \leq queryAdj[q].length\}$ ;
17       while  $cans$  is not empty do
18          $q \leftarrow \tau[cans.first]$ ;
19          $k \leftarrow 0$ ;
20          $cans \leftarrow cans \setminus cans.first$ ;
21         while  $k < targetAdj[q].length$  do
22           if ( $targetAdj[q][k] \neq -1$  or  $targetAdj[k][q] \neq -1$ )
23             and not  $\tau.contains(k)$  then
24                $\tau[q] \leftarrow k$ ;
25               break;
26            $k \leftarrow k + 1$ ;
27         if  $k \neq targetAdj[q].length$  then
28           break;
29 return result;

```

mapped nodes is 4. Next, we demonstrate how τ_0 is completed. We add all unmapped nodes to the queue Q . In this example, $Q = \{q_1\}$. Then we loop until Q is empty. We pop the first element q of Q , get the adjacency matrix of the query graph and the target graph, and traverse the adjacency matrix. We put the nodes q_m adjacent to q into the candidate nodes list $cans$, which is sorted by the connectivity of q_m and q . We get $cans = \{q_3, q_2, q_4, q_0\}$. Thereafter, we traverse $cans$ and take out of the first element q_3 in $cans$, and calculate the physical node $\mathbf{q} = \mathbf{q}_5$, $\tau_0(q_3) = \mathbf{q}_5$. Finally, we map q to the node connected to \mathbf{q} but not yet mapped. If the nodes connected to \mathbf{q} have been mapped, the loop continues. In this example, it can be directly mapped to \mathbf{q}_0 . In the end, we obtain the mapping

$$\tau_0 = \{q_0 \rightarrow \mathbf{q}_{10}, q_1 \rightarrow \mathbf{q}_0, q_2 \rightarrow \mathbf{q}_6, q_3 \rightarrow \mathbf{q}_5, q_4 \rightarrow \mathbf{q}_{11}\}.$$

4.3 Adjustment

Tabu search The Tabu search algorithm is a type of heuristic algorithm. It uses a tabu list to avoid searching repeated spaces, thereby avoiding deadlock. The algorithm uses amnesty rules to jump out of the local optimum to ensure the diversity of transformed results. The circuit adjustment mainly relies on the Tabu search algorithm, aiming to deal with those large circuits that the current algorithm is difficult to handle and produce an output circuit closer to the optimum solution.

The following objects are defined in Tabu search: neighborhoods, neighborhood action, tabu list, candidate set, tabu object, evaluation function, and amnesty rule. All the edges that can be swapped in the current map are the neighborhoods. The tabu list avoids local optimum and guarantees the parallelism of auxiliary gates. The tabu object is the object in the tabu list. We try not to use the recently swapped qubits as much as possible, which are added to the tabu list. We perform pruning to reduce search space, because only swaps adjacent to at least one gate node are meaningful. We select the edge in the shortest path that has an intersection with the qubits contained in the gate as the candidate set. The evaluation function selects a SWAP evaluation formula from the candidate set, taking the objective function as the evaluation function in general. The evaluation function should meet the requirements of some gates, and the number of SWAP gates added or the depth of the entire circuit should be small. The amnesty rules are used when all objects in the candidate set are banned, or after banning an object, the target value will be greatly reduced.

The calculation of the neighborhoods is shown in Algorithm 2. The input is the current circuit mapping τ_p . The variable *qubits* contains the mapping of physical qubits to logical qubits, where $j = \text{qubits}[i]$ means that the i -th physical qubit has been mapped to the j -th logical qubit. The variable *locations* represents the mapping of logical qubits to physical qubits, where $j = \text{locations}[i]$ means that the i -th logical qubit has been mapped to the j -th physical qubit. The current layer list of all gates is *cl*, and the output is a candidate set of the current mapping. The set E contains the edges of all the shortest paths in the

Algorithm 2: Calculate the candidate sets

Input: *dist*: The shortest paths of physical architecture
qubits: The mapping from physical qubits to logical qubits
locations: The mapping from logical qubits to physical qubits
cl: Gates included in the current layer of circuits
Output: *results*: The set of candidate solution

```

1 Initialize results  $\leftarrow \emptyset$ ;
2  $E_w \leftarrow$  Calculate the weight of each edge
3 swap_nodes  $\leftarrow$  An empty set of candidate swap nodes
4 foreach  $g \in cl$  do
5   if  $g$  is executable then
6      $cl \leftarrow cl \setminus \{g\}$ ;
7   else
8      $q_1 \leftarrow locations[g.control]$ ;
9      $q_2 \leftarrow locations[g.target]$ ;
10    swap_nodes.add( $q_1$ );
11    swap_nodes.add( $q_2$ );
12 foreach  $g \in cl$  do
13    $q_1 \leftarrow locations[g.control]$ ;
14    $q_2 \leftarrow locations[g.target]$ ;
15   foreach  $path \in paths[q_1][q_2]$  do
16     foreach  $e \in path$  do
17       if  $\{sour\_node, tar\_node\} \cap swap\_nodes \neq \emptyset$  then
18         new_qubits  $\leftarrow qubits$ ;
19         new_locations  $\leftarrow locations$ ;
20          $q_1 \leftarrow new\_qubits[e.source]$ ;
21          $q_2 \leftarrow new\_qubits[e.target]$ ;
22         new_qubits[ $e.source$ ]  $\leftarrow q_2$ ;
23         new_qubits[ $e.target$ ]  $\leftarrow q_1$ ;
24         if  $q_1 \neq -1$  then
25            $new\_locations[q_1] \leftarrow q_2$ ;
26         if  $q_2 \neq -1$  then
27            $new\_locations[q_2] \leftarrow q_1$ ;
28          $s \leftarrow \emptyset$ ;
29          $s.swaps \leftarrow p.swaps \cup \{distance.paths[path\_index][j]\}$ ;
30          $s.value \leftarrow compute\_evaluate\_value(dist, new\_locations, cl)$ ;
31         results  $\leftarrow results \cup \{s\}$ ;
32 return results;

```

physical architecture graph of all the gates in the current layer. Lines 17-31 swap all the edges of candidate set, and calculate the cost of them.

Example 4. Let us consider the mapping

$$\tau_0 = \{q_0 \rightarrow q_{10}, q_1 \rightarrow q_0, q_2 \rightarrow q_6, q_3 \rightarrow q_5, q_4 \rightarrow q_{11}\},$$

for $L_0 = \{g_0, g_1\}$, $dist_{cnot}(g_0) = 3$ and $dist_{cnot}(g_1) = 3$. Gate g_1 can be executed directly in the τ_0 mapping, so we delete it from L_0 , but g_0 cannot be executed in the mapping τ_0 . Thus, a circuit adjustment is required. Nodes that cannot be executed join the set $swap_nodes = \{q_0, q_6\}$. The set of shortest paths is $paths = \{\{q_6 \rightarrow q_1 \rightarrow q_0\}, \{q_6 \rightarrow q_5 \rightarrow q_0\}\}$, and then we traverse the shortest paths to calculate the candidate set. The two endpoints of an edge passed by one of the shortest paths should intersect with the swap set and join the candidate set. The current candidate set is $\{SWAP(q_6, q_1), SWAP(q_1, q_0), SWAP(q_6, q_5), SWAP(q_5, q_0)\}$.

Algorithm 3: Tabu search

Input: τ_{ini} : The initial mapping
 tl : Tabu list
Output: τ_{best} : The best mapping

```

1 Initialize  $\tau_{best} \leftarrow \tau_{ini}$ ;
2  $iter \leftarrow 1$ ; // Number of iterations
3 while not mustStop( $iter, \tau_{best}$ ) do
4    $C \leftarrow \tau_{ini}.candidates()$ ; // candidate set
5   if  $C$  is empty then
6      $\perp$  break;
7    $C_{best} \leftarrow find\_best\_candidates(C, tl)$ ;
8   if  $C_{best}$  is empty then
9      $\perp$   $C_{best} \leftarrow find\_amnesty\_candidates(C, tl)$ ;
10   $\tau_{best} \leftarrow C_{best}$ ;
11   $tl \leftarrow tl \cup \{C_{best}.swap\}$ ;
12   $iter \leftarrow iter + 1$ ;
13 return  $\tau_{best}$ 

```

The circuit mapping algorithm based on Tabu search takes a layered circuit and an initial mapping as input and outputs a circuit that can be executed in the specified architecture graph, as shown in Algorithm 3. The transformed circuit mapping of each layer is used as the initial mapping of the next layer. Line 1 regards the initial mapping τ_{ini} as the best mapping τ_{best} . Lines 3-12 cyclically check whether all gates in the current layer can be executed under the mapping τ_{ini} . If not all the gates are executable or the number of iterations has not reached the given maximum number, the search will continue. Otherwise,

the search will terminate. Line 4 gets the current mapping candidate, and Line 7 finds the best mapping in the candidate set. The mapping will first remove the overlapping elements of the candidate set and the tabu list. Then from the remaining candidates, we choose a mapping with the lowest cost. Line 9 are the amnesty rules. When the best candidate is not found, the candidate set elements are all the same as the tabu list elements. The amnesty rules select the mapping with the lowest cost in the candidate set as the best candidate mapping. Lines 10-12 update the best mapping τ_{best} and the current mapping τ_{curr} , and add the SWAP performed by the best mapping to the tabu list tl , indicating that the SWAP has just been performed. The algorithm would try to avoid re-swapping the just swapped qubits. Then it will check whether the termination condition of the algorithm is satisfied. The condition determines whether the number of iterations has reached the maximum number, or the current mapping ensures all gates in the current layer can be executed.

Example 5. Let us continue the previous example. We start searching from the initial mapping. We need to get the candidate SWAP set and select the one with the lower evaluation scores. For $L_0 = \{g_0, g_1\}$, the candidate set is

$$\{SWAP(q_6, q_1), SWAP(q_1, q_0), SWAP(q_6, q_5), SWAP(q_5, q_0)\},$$

and the costs are given as follows.

$$\begin{aligned} cost(SWAP(q_6, q_1)) &= 3.0, & cost(SWAP(q_1, q_0)) &= 3.0, \\ cost(SWAP(q_6, q_5)) &= 3.0, & cost(SWAP(q_5, q_0)) &= 3.0. \end{aligned}$$

The algorithm will choose the first SWAP, the mapping becomes

$$\tau_0 = \{q_0 \rightarrow q_{10}, q_1 \rightarrow q_0, q_2 \rightarrow q_1, q_3 \rightarrow q_5, q_4 \rightarrow q_{11}\}.$$

It can be seen that the current mapping ensures the executability of g_0 . The algorithm continues to search for the next layer.

Evaluation functions We can control the search direction by changing the evaluation functions. We test two evaluation functions: one uses the number of auxiliary gates in the generated circuit as the evaluation criterion (1), and the other uses the depth of the generated circuit as the evaluation criterion (2).

$$cost(SWAP(q_m, q_n)) = \sum_{g \in L} (dist[\tau(g.control)][\tau(g.target)]) \quad (1)$$

$$cost(SWAP(q_m, q_n)) = Depth(L) \quad (2)$$

Here $cost(SWAP(q_m, q_n))$ represents the cost of executing all the gates of the current layer L after swapping q_m with q_n . We only calculate the depth between the unmapped gates as in (1) or the distance of the unmapped gates as in (2).

Look ahead We observe that the number of gates in each layer after layering is small. The output of the i -th ($i < n$) layer is used as the input of the $(i+1)$ -th layer. Note that any swap operation in the i -th layer will affect the mapping of the $(i+1)$ -th layer. If we only consider the gates in the current layer when choosing the swapping gates, the swap only satisfies the requirement of the i -th layer, not necessarily the next layer. Therefore, we take the gates in the $(i+x)$ -th ($i+x < n$) layer into consideration, where x is the number of forward-looking layers. However, it is necessary to give a higher priority to the execution of the gates in the i -th layer, so we introduce an attenuation factor δ , which controls the influence of the gates in the $(i+x)$ -th layer. Heuristics show that for $x = 2$, $\delta = 0.9$, the final effect is approximately the best. Our evaluation functions in (1) and (2) can be adjusted as (3) and (4), respectively.

$$\begin{aligned} cost(SWAP(q_m, q_n)) = & \sum_{g \in L_i} (dist[\tau(g.control)][\tau(g.target)]) + \\ & \delta \times \sum_{j=i}^{i+x} \sum_{g \in L_j} (dist[\tau(g.control)][\tau(g.target)]) \end{aligned} \quad (3)$$

$$cost(SWAP(q_m, q_n)) = Depth(L_i) + \delta \times Depth(\sum_{j=i}^{i+x} L_j). \quad (4)$$

Complexity Given a logical circuit architecture graph $\mathcal{AG}_L = (V_L, E_L)$ and a physical circuit architecture graph $\mathcal{AG}_P = (V_P, E_P)$, we assume that the initial mapping is τ , the depth of the circuit is d , and the number of qubits is V_L . Tabu search deals with one layer at a time, and searches at most d times. Starting from the initial mapping, we first delete the executable gates of the first layer under the initial mapping. Then, the edges of all the shortest paths of all the gates that are not executable in the current layer are added to the candidate set where at least one node is in the gate mapping. In the worst case, the length of the shortest path is $(|E_P| - 1)$ and the size of the candidate set is $(|E_P| - 1)$. Each SWAP will make the total distance between the gates smaller. In the worst case, the number of SWAPs is $(|E_P| - 1)^{|E_P| - 2}$, but our selection strategy will make the number of SWAPs significantly reduced. The time complexity in the worst case is $d \times (|E_P| - 1)^{(|E_P| - 2)}$, and the space complexity is the size of our candidate set $(E_P - 1)$.

5 Experiments

We compare the CSIC algorithm and the circuit adjustment algorithm based on Tabu search TSA with the wghtgraph in [10] and the heuristic algorithm A^* in [25]. All the experiments are conducted on a Windows machine with 3.3GHz CPU and 10G memory.

First, we compare the efficiency of initial mapping on optm [25], CSIC and wghtgraph [10]. In order to observe the results of these two initial mapping

algorithms, we used the same circuit adjustment algorithm A^* [25]. We have tested 159 circuits. Within five minutes, *optm*, *wgtgraph*, and *CSIC* can deal with 121, 106, and 131 circuits, respectively. There are 103 circuits that they can handle. We then compare the *wgtgraph* algorithm and the *CSIC* algorithm more closely. The *wgtgraph* algorithm has 21 circuits with fewer auxiliary gates and 19 circuits with smaller depths, and the *CSIC* algorithm has 54 circuits with fewer auxiliary gates and 60 circuits with smaller depths. They output 25 circuits with equal depth and 29 circuits with equal auxiliary gates. On average, the auxiliary gates of the *CSIC* algorithm are reduced by 22.44%, and the depths are reduced by 11.25%.

Next, we compare the *optm* algorithm with the *CSIC* algorithm. The *optm* algorithm has one circuit with fewer auxiliary gates and two circuits with a small depth, while the *CSIC* algorithm has 99 circuits with fewer auxiliary gates and 98 circuits with a small depth. They have 4 circuits with equal depth and 4 circuits with equal auxiliary gates. The auxiliary gates of the *CSIC* algorithm are relatively reduced by 27.02%, and the depths are reduced by 14.12%. Table 1 shows the experimental data on 104 circuits. The three initial mapping algorithms are compared according to the depths of the generated circuits using the same A^* algorithm, and the numbers of added auxiliary gates. The column headed by *CSIC* /*optm* shows the efficiency improvement of the former upon the latter $(n_{optm} - n_{CSIC})/n_{optm}$.

| | optm | wgtgraph | CSIC | CSIC /optm | CSIC /wgtgraph |
|-----------------|--------|----------|--------|------------|----------------|
| Depths | 168895 | 163422 | 145040 | 14.12% | 11.25% |
| Auxiliary gates | 20439 | 19232 | 14916 | 27.02% | 22.44% |

Table 1. Compare *optm*, *wgtgraph*, and *CSIC* .

We then compare the use of two indicators TSA_{dep} and TSA_{num} that prioritize smaller depths and fewer auxiliary gates, respectively. Using the two indicators as objective functions, we tested 159 circuits. The depths of the final circuits obtained by TSA_{num} are 1.93% smaller than TSA_{dep} on average, and the numbers of auxiliary gates added are 4.53% smaller on average. When inserting a SWAP gate, the circuit needs to add 3 CNOT gates, and the depth will be increased by 3. Therefore, if fewer SWAP gates are added, the depths of the circuits will reduce accordingly.

Finally, we compare *TSA* with *wgtgraph*. Since the *wgtgraph* algorithm only uses 2-qubit gates, it is impossible to compare the depths of the generated circuits. Instead, we compare the number of SWAP gates added and the time costs. We set a five-minute timeout period and tested 159 circuits. It turns out that TSA_{num} only takes 461 seconds and TSA_{dep} takes 485 seconds. The *wgtgraph* algorithm takes 1908 seconds for the 159 circuits, but only produces valid results for 99 circuits, including 64 small circuits, 35 medium-sized circuits, and no circuit output is produced for any of the 44 large circuits. Although Tabu

search can quickly produce results on large circuits, in contrast, more auxiliary gates are added. In the generated circuits obtained by wgtgraph from 99 small and medium-sized circuits, the number of SWAP gates added by wgtgraph is 26.87% (resp. 24.89%) smaller than TSA_{num} (resp. TSA_{dep}) on average. The Tabu search can quickly output converted circuits on large circuits, but wgtgraph cannot get results in the predefined time bound. Since our candidate set is too small to be able to process the circuit quickly, but this also leads to an increase in the insertion of additional gates. As to SABRE, when dealing with 159 circuits with a five-minute limit for each circuit, it successfully produces results for only 23 small circuits, 6 medium-sized circuits, and 1 large circuit. The detailed results of the circuit comparisons are in the Appendix.

| benchmarks | #circ. | TSA_{num} | | TSA_{dep} | | wgtgraph | | SABRE | |
|------------|--------|-------------|------|-------------|------|----------|------|--------|---------|
| | | #succ. | time | #succ. | time | #succ. | time | #succ. | time |
| small | 66 | 66 | 32 | 66 | 29 | 64 | 587 | 23 | 12996 |
| medium | 49 | 49 | 45 | 49 | 40 | 35 | 1183 | 6 | 13019 |
| large | 44 | 44 | 407 | 44 | 432 | 0 | - | 0 | 1340719 |
| total | 159 | 159 | 484 | 159 | 501 | 99 | - | 29 | 1366734 |

Table 2. Compare optm, wgtgraph, SABRE TSA_{num} and TSA_{dep} .

6 Conclusion

We propose a scalable algorithm for quantum circuit transformation. First, we use a subgraph isomorphism algorithm and a mapping completion method based on the connectivity between qubits to generate a high-quality initial mapping. Secondly we exploit a look-ahead heuristic search taking into account the influence of the pre-layer circuit mapping to reduce the number of auxiliary gates, and complete the transformation. Finally, we compare the influence of initial mapping with the state-of-the-art algorithm wgtgraph and optm and also compare the overall efficiency with optm, wgtgraph, and SABRE. Experimental results show that the initial mapping generated by CSIC have fewer SWAP gates inserted and the results can be obtained in an acceptable amount of time. Most small and medium-sized circuits can be handled in a few seconds. For large circuits, the results can be obtained within a few minutes, but the cost of insertion may be larger than that of wgtgraph. We introduce a look-ahead method to make each selected SWAP more in line with the constraints of the gates to be processed. In the future, we will investigate how to reduce the number of inserted auxiliary gates and increase the speed. We will also apply the proposed method to more NISQ devices.

References

1. Almeida, A., Dueck, G., Silva, A.: Finding optimal qubit permutations for ibm’s quantum computer architectures pp. 1–6 (08 2019). <https://doi.org/10.1145/3338852.3339829>
2. Barenco, A., Bennett, C., Cleve, R., DiVincenzo, D., Margolus, N., Shor, P., Sleator, T., Smolin, J., Weinfurter, H.: Elementary gates for quantum computation. *Physical Review A* **52** (03 1995). <https://doi.org/10.1103/PhysRevA.52.3457>
3. Bernal, D., Booth, K., Dridi, R., Alghassi, H., Tayur, S., Venturelli, D.: Integer programming techniques for minor-embedding in quantum annealers (12 2019)
4. Cowtan, A., Dilkes, S., Duncan, R., Krajenbrink, A., Simmons, W., Sivarajah, S.: On the qubit routing problem (02 2019)
5. Daei, O., Navi, K., Zomorodi, M.: Optimized quantum circuit partitioning (05 2020)
6. Glover, F.: Tabu search—part ii. *ORSA Journal on Computing* **2**, 4–32 (02 1990). <https://doi.org/10.1287/ijoc.2.1.4>
7. Guerreschi, G.G., Park, J.: Two-step approach to scheduling quantum circuits. *Quantum Science and Technology* **3** (06 2018). <https://doi.org/10.1088/2058-9565/aacf0b>
8. Kissinger, A., Meijer, A.: Cnot circuit extraction for topologically-constrained quantum memories (04 2019)
9. Li, G., Ding, Y., Xie, Y.: Tackling the qubit mapping problem for nisq-era quantum devices (09 2018)
10. Li, S., Zhou, X., Feng, Y.: Qubit mapping based on subgraph isomorphism and filtered depth-limited search (2020)
11. Matsuo, A., Yamashita, S.: An efficient method for quantum circuit placement problem on a 2-d grid pp. 162–168 (05 2019). https://doi.org/10.1007/978-3-030-21500-2_10
12. Murali, P., Linke, N., Martonosi, M., Abhari, A., Nguyen, N., Huerta Alderete, C.: Full-stack, real-system quantum computer studies: architectural comparisons and design insights pp. 527–540 (06 2019). <https://doi.org/10.1145/3307650.3322273>
13. Möttönen, M., Vartiainen, J.: Decompositions of general quantum gates. *Frontiers in Artificial Intelligence and Applications* (05 2005)
14. Nash, B., Gheorghiu, V., Mosca, M.: Quantum circuit optimizations for nisq architectures. *Quantum Science and Technology* **5** (02 2020). <https://doi.org/10.1088/2058-9565/ab79b1>
15. Paler, A.: On the influence of initial qubit placement during nisq circuit compilation (11 2018)
16. Preskill, J.: Quantum computing in the nisq era and beyond. *Quantum* **2** (2018)
17. Shafaei, A., Saeedi, M., Pedram, M.: Optimization of quantum circuits for interaction distance in linear nearest neighbor architectures. *Proceedings - Design Automation Conference* pp. 1–6 (05 2013). <https://doi.org/10.1145/2463209.2488785>
18. Shafaei, A., Saeedi, M., Pedram, M.: Optimization of quantum circuits for interaction distance in linear nearest neighbor architectures (2013)
19. Siraichi, M.Y., dos Santos, V.F., Collange, S., Pereira, F.M.Q.: Qubit allocation (2018)
20. Sun, S., Luo, Q.: In-memory subgraph matching: An in-depth study pp. 1083–1098 (06 2020). <https://doi.org/10.1145/3318464.3380581>
21. Tannu, S., Qureshi, M.: Not all qubits are created equal: A case for variability-aware policies for nisq-era quantum computers pp. 987–999 (04 2019). <https://doi.org/10.1145/3297858.3304007>

22. Venturelli, D., do, M., Rieffel, E., Frank, J.: Temporal planning for compilation of quantum approximate optimization circuits pp. 4440–4446 (08 2017). <https://doi.org/10.24963/ijcai.2017/620>
23. Xiangzhen, Z., Li, S., Feng, Y.: Quantum circuit transformation based on simulated annealing and heuristic search. *IEEE Transactions on Computer-Aided Design of Integrated Circuits and Systems* **PP**, 1–1 (01 2020). <https://doi.org/10.1109/TCAD.2020.2969647>
24. Zhang, Y., Deng, H., Li, Q., Haoze, S., Nie, L.: Optimizing quantum programs against decoherence: Delaying qubits into quantum superposition pp. 184–191 (07 2019). <https://doi.org/10.1109/TASE.2019.000-2>
25. Zulehner, A., Paller, A., Wille, R.: Efficient mapping of quantum circuits to the ibm qx architectures. *IEEE Transactions on Computer-Aided Design of Integrated Circuits and Systems* (12 2017). <https://doi.org/10.1109/TCAD.2018.2846658>

A Experimental details of the SWAP gates added by the output circuits

| Circuit name | qubit no. | CNOT no. | TSA _{num} added | TSA _{dep} added | optm added | wghtgr added | SABRE added |
|----------------------|-----------|----------|--------------------------|--------------------------|------------|--------------|-------------|
| decod24-enable_126 | 6 | 149 | 28 | 42 | 60 | 16 | 129 |
| 4mod5-v0_19 | 5 | 16 | 0 | 0 | 0 | 0 | - |
| 4mod5-v0_18 | 5 | 31 | 2 | 5 | 4 | 4 | - |
| mod5d2_64 | 5 | 25 | 5 | 6 | 8 | 3 | - |
| 4gt4-v0_72 | 6 | 113 | 14 | 10 | 33 | 14 | - |
| alu-v3_35 | 5 | 18 | 2 | 4 | 8 | 2 | - |
| 4gt4-v0_73 | 6 | 179 | 27 | 34 | 76 | 12 | - |
| alu-v3_34 | 5 | 24 | 2 | 3 | 7 | 2 | - |
| 3_17_13 | 3 | 17 | 0 | 0 | 6 | 0 | 0 |
| 4gt4-v0_78 | 6 | 109 | 12 | 8 | 48 | 4 | 124 |
| 4gt4-v0_79 | 6 | 105 | 17 | 17 | 48 | 3 | - |
| 4mod7-v1_96 | 5 | 72 | 16 | 19 | 27 | 7 | - |
| mod10_171 | 5 | 108 | 17 | 20 | 39 | 9 | - |
| ex2_227 | 7 | 275 | 48 | 59 | 121 | 33 | - |
| mod10_176 | 5 | 78 | 14 | 14 | 38 | 8 | - |
| 0410184_169 | 5 | 9 | 2 | 2 | 49 | 3 | - |
| 4mod5-v0_20 | 5 | 10 | 0 | 0 | 4 | 0 | - |
| aj-e11_165 | 5 | 69 | 8 | 8 | 33 | 7 | 63 |
| alu-v1_28 | 5 | 18 | 2 | 4 | 11 | 2 | - |
| 4gt12-v0_86 | 6 | 116 | 28 | 33 | 48 | 3 | - |
| 4gt12-v0_87 | 6 | 112 | 27 | 32 | 45 | 2 | - |
| 4gt12-v0_88 | 6 | 86 | 5 | 5 | 25 | 4 | - |
| alu-v1_29 | 5 | 17 | 4 | 4 | 11 | 2 | 13 |
| ham7_104 | 7 | 149 | 28 | 34 | 68 | 12 | - |
| C17_204 | 7 | 205 | 26 | 53 | 99 | 22 | - |
| xor5_254 | 6 | 5 | 0 | 0 | 1 | 0 | 3 |
| hwb4_49 | 5 | 107 | 14 | 15 | 38 | 11 | 157 |
| rd73_140 | 10 | 104 | 23 | 26 | 35 | 20 | - |
| decod24-v0_38 | 4 | 23 | 0 | 0 | 6 | 0 | - |
| rd53_131 | 7 | 200 | 39 | 39 | 98 | 24 | - |
| rd53_133 | 7 | 256 | 37 | 47 | 102 | 27 | 160 |
| rd53_135 | 7 | 134 | 28 | 29 | 38 | 23 | - |
| decod24-v2_43 | 4 | 22 | 0 | 0 | 9 | 0 | 39 |
| rd53_138 | 8 | 60 | 14 | 16 | 23 | 9 | - |
| rd32-v0_66 | 4 | 16 | 0 | 0 | 6 | 0 | - |
| 4gt13-v1_93 | 5 | 30 | 0 | 0 | 13 | 0 | - |
| graycode6_47 | 6 | 5 | 0 | 0 | 0 | 0 | - |
| 4mod5-bdd_287 | 7 | 31 | 3 | 6 | 8 | 6 | 34 |
| ham3_102 | 3 | 11 | 0 | 0 | 3 | 0 | 12 |
| 4gt4-v0_80 | 6 | 79 | 5 | 5 | 22 | 5 | - |
| ex-1_166 | 3 | 9 | 0 | 0 | 3 | 0 | - |
| mod5mils_65 | 5 | 16 | 0 | 0 | 6 | 0 | - |
| 0example | 5 | 9 | 1 | 2 | 3 | 3 | - |
| alu-v4_36 | 5 | 51 | 12 | 8 | 22 | 4 | 41 |
| alu-v4_37 | 5 | 18 | 2 | 4 | 8 | 2 | - |
| ex1_226 | 6 | 5 | 0 | 0 | 1 | 0 | 15 |
| one-two-three-v0_98 | 5 | 65 | 11 | 13 | 32 | 10 | - |
| one-two-three-v0_97 | 5 | 128 | 23 | 23 | 64 | 16 | - |
| one-two-three-v3_101 | 5 | 32 | 3 | 4 | 14 | 3 | - |
| rd32_270 | 5 | 36 | 3 | 3 | 6 | 6 | 24 |

Table 3. Comparison of the number of SWAP gates added by the output circuit on the IBM Q20

| Circuit name | qubit no. | CNOT no. | TSA _{num} added | TSA _{dep} added | optm added | wghtgr added | SABRE added |
|----------------------|-----------|----------|--------------------------|--------------------------|------------|--------------|-------------|
| rd53_130 | 7 | 448 | 89 | 100 | 190 | 49 | - |
| rd53_251 | 8 | 564 | 104 | 131 | 230 | 45 | - |
| 4mod5-v1_24 | 5 | 16 | 0 | 0 | 3 | 0 | - |
| mod5adder_127 | 6 | 239 | 21 | 56 | 111 | 20 | - |
| 4_49_16 | 5 | 99 | 20 | 17 | 40 | 10 | - |
| hwb5_53 | 6 | 598 | 141 | 168 | 173 | 59 | - |
| ex3_229 | 6 | 175 | 10 | 9 | 50 | 11 | - |
| 4gt10-v1_81 | 5 | 66 | 14 | 15 | 28 | 6 | - |
| alu-v2_32 | 5 | 72 | 15 | 17 | 27 | 7 | - |
| alu-v2_31 | 5 | 198 | 42 | 54 | 85 | 13 | - |
| alu-v2_30 | 6 | 223 | 41 | 45 | 96 | 20 | - |
| sf_276 | 6 | 336 | 12 | 52 | 138 | 12 | - |
| decod24-v1_41 | 5 | 38 | 4 | 4 | 14 | 3 | 28 |
| sf_274 | 6 | 336 | 34 | 21 | 82 | 12 | - |
| 4gt4-v1_74 | 6 | 119 | 17 | 24 | 37 | 9 | - |
| alu-v2_33 | 5 | 17 | 4 | 4 | 8 | 2 | - |
| cnt3-5_179 | 16 | 85 | 6 | 6 | 35 | 4 | - |
| 4mod5-v1_22 | 5 | 11 | 0 | 0 | 5 | 0 | 0 |
| 4mod5-v1_23 | 5 | 32 | 5 | 5 | 4 | 3 | 55 |
| mini_alu_305 | 10 | 77 | 10 | 20 | 28 | 8 | 123 |
| alu-v0_26 | 5 | 38 | 7 | 10 | 13 | 3 | - |
| alu-bdd_288 | 7 | 38 | 4 | 12 | 16 | 6 | - |
| alu-v0_27 | 5 | 17 | 2 | 4 | 11 | 2 | 9 |
| 4gt13_91 | 5 | 49 | 7 | 7 | 10 | 2 | - |
| 4gt5_77 | 5 | 58 | 12 | 12 | 20 | 6 | - |
| 4gt13_92 | 5 | 30 | 0 | 0 | 14 | 0 | - |
| 4gt5_76 | 5 | 46 | 7 | 10 | 24 | 5 | 39 |
| 4gt5_75 | 5 | 38 | 5 | 12 | 16 | 4 | 53 |
| 4gt12-v1_89 | 6 | 100 | 11 | 21 | 38 | 4 | - |
| one-two-three-v1_99 | 5 | 59 | 12 | 10 | 26 | 7 | - |
| 4gt13_90 | 5 | 53 | 7 | 7 | 13 | 3 | - |
| ising_model_10 | 10 | 90 | 0 | 0 | 5 | 0 | - |
| 4gt11_84 | 5 | 9 | 0 | 0 | 3 | 0 | 12 |
| 4gt11_83 | 5 | 14 | 0 | 0 | 0 | 0 | - |
| mod5d1_63 | 5 | 13 | 0 | 0 | 1 | 0 | - |
| 4gt11_82 | 5 | 18 | 1 | 1 | 1 | 1 | - |
| decod24-v3_45 | 5 | 64 | 15 | 15 | 32 | 8 | 64 |
| rd32-v1_68 | 4 | 16 | 0 | 0 | 6 | 0 | 24 |
| mini_alu_167 | 5 | 126 | 27 | 27 | 49 | 11 | - |
| one-two-three-v2_100 | 5 | 32 | 3 | 4 | 8 | 3 | - |
| 4mod7-v0_94 | 5 | 72 | 8 | 13 | 36 | 9 | - |
| cm82a_208 | 8 | 283 | 41 | 69 | 84 | 33 | - |
| mod8-10_178 | 6 | 152 | 5 | 20 | 13 | 7 | - |
| mod8-10_177 | 6 | 196 | 14 | 33 | 58 | 13 | 230 |
| majority_239 | 7 | 267 | 39 | 43 | 105 | 33 | - |
| miller_11 | 3 | 23 | 0 | 0 | 9 | 0 | 36 |
| decod24-bdd_294 | 6 | 32 | 4 | 4 | 9 | 4 | 36 |
| total | 551 | 9244 | 1372 | 1738 | 3481 | 800 | - |

Table 4. Comparison of the number of SWAP gates added by the output circuit on the IBM Q20

| Circuit name | qubit no. | CNOT no. | TSA _{num} added | TSA _{dep} added | optm added | wghtgr added | SABRE added |
|----------------------------|--------------|-------------|-----------------------------|-----------------------------|---------------|-----------------|----------------|
| max46_240 | 10 | 11844 | 3473 | 4545 | - | - | - |
| rd73_252 | 10 | 2319 | 586 | 761 | - | - | - |
| cycle10_2_110 | 12 | 2648 | 919 | 1216 | 961 | - | - |
| sqrt8_260 | 12 | 1314 | 379 | 492 | 457 | - | - |
| urf4_187 | 11 | 224028 | 54785 | 60140 | - | - | - |
| sqn_258 | 10 | 4459 | 1199 | 1420 | - | - | - |
| f2_232 | 8 | 525 | 87 | 124 | 218 | - | - |
| radd_250 | 13 | 1405 | 386 | 489 | 511 | - | - |
| ham15_107 | 15 | 3858 | 1326 | 1689 | - | - | - |
| sao2_257 | 14 | 16864 | 5346 | 7178 | - | - | - |
| sym9_148 | 10 | 9408 | 1865 | 2432 | - | - | - |
| urf5_280 | 9 | 23764 | 6989 | 8730 | - | - | - |
| square.root_7 | 15 | 3089 | 812 | 2150 | - | - | - |
| sys6-v0_111 | 10 | 98 | 23 | 26 | 38 | - | - |
| hwb7_59 | 8 | 10681 | 2687 | 3551 | 3722 | - | - |
| sym9_146 | 12 | 148 | 38 | 55 | 54 | - | 248 |
| wim_266 | 11 | 427 | 93 | 120 | 147 | - | - |
| urf2_152 | 8 | 35210 | 9181 | 11921 | 10577 | - | - |
| urf5_159 | 9 | 71932 | 20258 | 25505 | - | - | - |
| urf2_277 | 8 | 10066 | 2807 | 3798 | 3782 | - | - |
| life_238 | 11 | 9800 | 2762 | 3576 | - | - | - |
| root_255 | 13 | 7493 | 2128 | 3035 | - | - | - |
| 9symml_195 | 11 | 15232 | 4553 | 5986 | - | - | - |
| sym10_262 | 12 | 28084 | 8534 | 11033 | - | - | - |
| dc1_220 | 11 | 833 | 226 | 207 | 371 | - | - |
| cm42a_207 | 14 | 771 | 182 | 229 | 294 | - | - |
| rd53_311 | 13 | 124 | 26 | 48 | 47 | - | - |
| dc2_222 | 15 | 4131 | 1383 | 1773 | - | - | - |
| rd84_142 | 15 | 154 | 49 | 58 | 50 | - | - |
| sym6_145 | 7 | 1701 | 317 | 449 | 750 | - | - |
| co14_215 | 15 | 7840 | 3078 | 3819 | - | - | - |
| cnt3-5_180 | 16 | 215 | 59 | 74 | 79 | - | - |
| cm152a_212 | 12 | 532 | 103 | 129 | 168 | - | - |
| sym6_316 | 14 | 123 | 30 | 39 | 56 | - | - |
| mlp4_245 | 16 | 8232 | 2780 | 3490 | - | - | - |
| hwb8_113 | 9 | 30372 | 10749 | 16489 | - | - | - |
| qft_16 | 16 | 240 | 90 | 147 | - | - | - |
| plus63mod4096_163 | 13 | 56329 | 19759 | 24273 | - | - | - |
| urf1_149 | 9 | 80878 | 22551 | 28516 | - | - | - |
| urf3_155 | 10 | 185276 | 50842 | 62903 | - | - | - |
| urf3_279 | 10 | 60380 | 17999 | 23318 | - | - | - |
| hwb9_119 | 10 | 90955 | 22946 | 30031 | - | - | - |
| plus63mod8192_164 | 14 | 81865 | 28022 | 36207 | - | - | - |
| pm1_249 | 14 | 771 | 182 | 229 | 294 | - | - |
| sym9_193 | 11 | 15232 | 4382 | 5518 | - | - | - |
| misex1_241 | 15 | 2100 | 480 | 754 | 600 | - | - |
| urf1_278 | 9 | 26692 | 8010 | 10217 | - | - | - |
| squar5_261 | 13 | 869 | 219 | 313 | 290 | - | - |
| ground_state_estimation_10 | 13 | 154209 | 11671 | 22886 | - | - | - |
| adr4_197 | 13 | 1498 | 516 | 670 | - | - | - |

Table 5. Comparison of the number of SWAP gates added by the output circuit on the IBM Q20

| Circuit name | qubit no. | CNOT no. | TSA _{num} added | TSA _{dep} added | optm added | wghtgr added | SABRE added |
|-----------------|--------------|-------------|-----------------------------|-----------------------------|---------------|-----------------|----------------|
| hwb6_56 | 7 | 2952 | 698 | 933 | 909 | - | - |
| clip_206 | 14 | 14772 | 5430 | 6865 | - | - | - |
| cm85a_209 | 14 | 4986 | 2088 | 2225 | - | - | - |
| rd84_253 | 12 | 5960 | 1849 | 2333 | - | - | - |
| dist_223 | 13 | 16624 | 5623 | 7431 | - | - | - |
| inc_237 | 16 | 4636 | 1193 | 1667 | - | - | - |
| qft_10 | 10 | 90 | 23 | 34 | 30 | - | - |
| urf6_160 | 15 | 75180 | 27524 | 32452 | - | - | - |
| con1_216 | 9 | 415 | 86 | 118 | 177 | - | - |

Table 6. Comparison of the number of SWAP gates added by the output circuit on the IBM Q20

B Experimental details of the depths of the output circuits

| Circuit name | qubit no. | CNOT no. | depths no. | TSA _{num} depths | TSA _{dep} depths | optm depths |
|--------------------|-----------|----------|------------|---------------------------|---------------------------|-------------|
| decod24-enable_126 | 6 | 149 | 190 | 233 | 275 | 470 |
| 4mod5-v0_19 | 5 | 16 | 21 | 16 | 16 | 21 |
| 4mod5-v0_18 | 5 | 31 | 40 | 37 | 46 | 54 |
| mod5d2_64 | 5 | 25 | 32 | 40 | 43 | 67 |
| 4gt4-v0_72 | 6 | 113 | 137 | 155 | 143 | 297 |
| alu-v3_35 | 5 | 18 | 22 | 24 | 30 | 60 |
| 4gt4-v0_73 | 6 | 179 | 227 | 260 | 281 | 586 |
| alu-v3_34 | 5 | 24 | 30 | 30 | 33 | 63 |
| 3_17_13 | 3 | 17 | 22 | 17 | 17 | 52 |
| 4gt4-v0_78 | 6 | 109 | 137 | 145 | 133 | 352 |
| 4gt4-v0_79 | 6 | 105 | 132 | 156 | 156 | 345 |
| 4mod7-v1_96 | 5 | 72 | 94 | 120 | 129 | 218 |
| mod10_171 | 5 | 108 | 139 | 159 | 168 | 335 |
| ex2_227 | 7 | 275 | 355 | 419 | 452 | 899 |
| mod10_176 | 5 | 78 | 101 | 120 | 120 | 104 |
| cycle10_2_110 | 12 | 2648 | 3386 | 5405 | 6296 | 7467 |
| 0410184_169 | 5 | 9 | 6 | 15 | 15 | 253 |
| 4mod5-v0_20 | 5 | 10 | 12 | 10 | 10 | 32 |
| sqrt8_260 | 12 | 1314 | 1661 | 2451 | 2790 | 3561 |
| aj-e11_165 | 5 | 69 | 86 | 93 | 93 | 250 |
| alu-v1_28 | 5 | 18 | 22 | 24 | 30 | 70 |
| f2_232 | 8 | 525 | 668 | 786 | 897 | 1672 |
| radd_250 | 13 | 1405 | 1781 | 2563 | 2872 | 3985 |
| 4gt12-v0_86 | 6 | 116 | 135 | 200 | 215 | 334 |
| 4gt12-v0_87 | 6 | 112 | 131 | 193 | 208 | 324 |
| 4gt12-v0_88 | 6 | 86 | 108 | 101 | 101 | 222 |
| alu-v1_29 | 5 | 17 | 22 | 29 | 29 | 64 |
| ham7_104 | 7 | 149 | 185 | 233 | 251 | 491 |
| C17_204 | 7 | 205 | 253 | 283 | 364 | 688 |
| xor5_254 | 6 | 5 | 5 | 5 | 5 | 10 |
| hwb4_49 | 5 | 107 | 134 | 149 | 152 | 308 |
| rd73_140 | 10 | 104 | 92 | 173 | 182 | 185 |
| decod24-v0_38 | 4 | 23 | 30 | 23 | 23 | 61 |
| rd53_131 | 7 | 200 | 261 | 317 | 317 | 677 |
| rd53_133 | 7 | 256 | 327 | 367 | 397 | 777 |
| rd53_135 | 7 | 134 | 159 | 218 | 221 | 331 |
| sys6-v0_111 | 10 | 98 | 75 | 167 | 176 | 188 |
| decod24-v2_43 | 4 | 22 | 30 | 22 | 22 | 75 |
| hwb7_59 | 8 | 10681 | 13437 | 18742 | 21334 | 29601 |
| rd53_138 | 8 | 60 | 56 | 102 | 108 | 114 |
| rd32-v0_66 | 4 | 16 | 20 | 16 | 16 | 51 |
| sym9_146 | 12 | 148 | 127 | 262 | 313 | 309 |
| 4gt13-v1_93 | 5 | 30 | 39 | 30 | 30 | 102 |
| graycode6_47 | 6 | 5 | 5 | 5 | 5 | 5 |
| wim_266 | 11 | 427 | 514 | 706 | 787 | 1180 |
| urf2_152 | 8 | 35210 | 44100 | 62753 | 70973 | 90299 |
| urf2_277 | 8 | 10066 | 11390 | 18487 | 21460 | 26548 |
| 4mod5-bdd_287 | 7 | 31 | 41 | 40 | 49 | 71 |
| ham3_102 | 3 | 11 | 13 | 11 | 11 | 28 |
| 4gt4-v0_80 | 6 | 79 | 101 | 94 | 94 | 206 |

Table 7. Comparison of the depth of the output circuit on the IBM Q20

| Circuit name | qubit no. | CNOT no. | depths no. | TSA _{num} depths | TSA _{dep} depths | optm depths |
|----------------------|--------------|-------------|---------------|------------------------------|------------------------------|----------------|
| ex-1.166 | 3 | 9 | 12 | 9 | 9 | 28 |
| mod5mils.65 | 5 | 16 | 21 | 16 | 16 | 52 |
| 0example | 5 | 9 | 6 | 12 | 15 | 15 |
| alu-v4.36 | 5 | 51 | 66 | 87 | 75 | 170 |
| alu-v4.37 | 5 | 18 | 22 | 24 | 30 | 60 |
| ex1.226 | 6 | 5 | 5 | 5 | 5 | 10 |
| one-two-three-v0.98 | 5 | 65 | 82 | 98 | 104 | 234 |
| one-two-three-v0.97 | 5 | 128 | 163 | 197 | 197 | 443 |
| one-two-three-v3.101 | 5 | 32 | 40 | 41 | 44 | 95 |
| rd32.270 | 5 | 36 | 47 | 45 | 45 | 76 |
| dc1.220 | 11 | 833 | 1041 | 1511 | 1454 | 2711 |
| rd53.130 | 7 | 448 | 569 | 715 | 748 | 1417 |
| rd53.251 | 8 | 564 | 712 | 876 | 957 | 1767 |
| cm42a.207 | 14 | 771 | 940 | 1317 | 1458 | 2279 |
| rd53.311 | 13 | 124 | 130 | 202 | 268 | 300 |
| 4mod5-v1.24 | 5 | 16 | 21 | 16 | 16 | 36 |
| mod5adder.127 | 6 | 239 | 302 | 302 | 407 | 817 |
| 4.49.16 | 5 | 99 | 125 | 159 | 150 | 320 |
| hwb5.53 | 6 | 598 | 758 | 1021 | 1102 | 1560 |
| ex3.229 | 6 | 175 | 226 | 205 | 202 | 462 |
| rd84.142 | 15 | 154 | 110 | 301 | 328 | 253 |
| 4gt10-v1.81 | 5 | 66 | 84 | 108 | 111 | 210 |
| alu-v2.32 | 5 | 72 | 92 | 117 | 123 | 215 |
| alu-v2.31 | 5 | 198 | 255 | 324 | 360 | 650 |
| alu-v2.30 | 6 | 223 | 285 | 346 | 358 | 734 |
| sym6.145 | 7 | 1701 | 2187 | 2652 | 3048 | 5716 |
| sf.276 | 6 | 336 | 435 | 372 | 492 | 1096 |
| decod24-v1.41 | 5 | 38 | 50 | 50 | 50 | 120 |
| sf.274 | 6 | 336 | 436 | 438 | 399 | 822 |
| 4gt4-v1.74 | 6 | 119 | 154 | 170 | 191 | 329 |
| alu-v2.33 | 5 | 17 | 22 | 29 | 29 | 59 |
| cnt3-5.180 | 16 | 215 | 209 | 392 | 437 | 482 |
| cm152a.212 | 12 | 532 | 684 | 841 | 919 | 1423 |
| cnt3-5.179 | 16 | 85 | 61 | 103 | 103 | 166 |
| sym6.316 | 14 | 123 | 135 | 213 | 240 | 378 |
| 4mod5-v1.22 | 5 | 11 | 12 | 11 | 11 | 37 |
| 4mod5-v1.23 | 5 | 32 | 41 | 47 | 47 | 55 |
| mini_alu.305 | 10 | 77 | 71 | 107 | 137 | 187 |
| alu-v0.26 | 5 | 38 | 49 | 59 | 68 | 108 |
| alu-bdd.288 | 7 | 38 | 48 | 50 | 74 | 112 |
| alu-v0.27 | 5 | 17 | 21 | 23 | 29 | 63 |
| 4gt13.91 | 5 | 49 | 61 | 70 | 70 | 108 |
| 4gt5.77 | 5 | 58 | 74 | 94 | 94 | 170 |
| 4gt13.92 | 5 | 30 | 38 | 30 | 30 | 103 |
| 4gt5.76 | 5 | 46 | 56 | 67 | 76 | 171 |
| 4gt5.75 | 5 | 38 | 47 | 53 | 74 | 127 |
| 4gt12-v1.89 | 6 | 100 | 130 | 133 | 163 | 313 |
| one-two-three-v1.99 | 5 | 59 | 76 | 95 | 89 | 194 |
| 4gt13.90 | 5 | 53 | 65 | 74 | 74 | 124 |
| pm1.249 | 14 | 771 | 940 | 1317 | 1458 | 2279 |

Table 8. Comparison of the depth of the output circuit on the IBM Q20

| Circuit name | qubit no. | CNOT no. | depths no. | TSA _{num} depths | TSA _{dep} depths | optm depths |
|----------------------|--------------|-------------|---------------|------------------------------|------------------------------|----------------|
| ising_model_10 | 10 | 90 | 52 | 90 | 90 | 107 |
| misex1_241 | 15 | 2100 | 2676 | 3540 | 4362 | 5326 |
| 4gt11_84 | 5 | 9 | 11 | 9 | 9 | 25 |
| 4gt11_83 | 5 | 14 | 16 | 14 | 14 | 16 |
| mod5d1_63 | 5 | 13 | 13 | 13 | 13 | 17 |
| 4gt11_82 | 5 | 18 | 20 | 21 | 21 | 25 |
| squar5_261 | 13 | 869 | 1051 | 1526 | 1808 | 2309 |
| decod24-v3_45 | 5 | 64 | 84 | 109 | 109 | 244 |
| rd32-v1_68 | 4 | 16 | 21 | 16 | 16 | 52 |
| hwb6_56 | 7 | 2952 | 3736 | 5046 | 5751 | 7773 |
| mini-alu_167 | 5 | 126 | 162 | 207 | 207 | 400 |
| one-two-three-v2_100 | 5 | 32 | 40 | 41 | 44 | 80 |
| 4mod7-v0_94 | 5 | 72 | 92 | 96 | 111 | 270 |
| cm82a_208 | 8 | 283 | 340 | 406 | 490 | 699 |
| mod8-10_178 | 6 | 152 | 193 | 167 | 212 | 243 |
| mod8-10_177 | 6 | 196 | 251 | 238 | 295 | 525 |
| majority_239 | 7 | 267 | 344 | 384 | 396 | 839 |
| qft_10 | 10 | 90 | 37 | 159 | 192 | 135 |
| millar_11 | 3 | 23 | 29 | 23 | 23 | 75 |
| decod24-bdd_294 | 6 | 32 | 40 | 44 | 44 | 86 |
| con1_216 | 9 | 415 | 508 | 673 | 769 | 1197 |
| total | 823 | 83416 | 103023 | 145372 | 164848 | 224731 |

Table 9. Comparison of the depth of the output circuit on the IBM Q20

| Circuit name | qubit no. | CNOT no. | depths no. | TSA _{num} depths | TSA _{dep} depths | optm depths |
|----------------------------|--------------|-------------|---------------|------------------------------|------------------------------|----------------|
| max46_240 | 10 | 11844 | 14257 | 22263 | 25479 | - |
| rd73_252 | 10 | 2319 | 2867 | 4077 | 4602 | - |
| urf4_187 | 11 | 224028 | 264330 | 388383 | 404448 | - |
| sqn_258 | 10 | 4459 | 5458 | 8056 | 8719 | - |
| ham15_107 | 15 | 3858 | 4819 | 7836 | 8925 | - |
| sao2_257 | 14 | 16864 | 19563 | 32902 | 38398 | - |
| sym9_148 | 10 | 9408 | 12087 | 15003 | 16704 | - |
| urf5_280 | 9 | 23764 | 27822 | 44731 | 49954 | - |
| square_root_7 | 15 | 3089 | 3847 | 5525 | 9539 | - |
| urf5_159 | 9 | 71932 | 89148 | 132706 | 148447 | - |
| life_238 | 11 | 9800 | 12511 | 18086 | 20528 | - |
| root_255 | 13 | 7493 | 8839 | 13877 | 16598 | - |
| 9symml_195 | 11 | 15232 | 19235 | 28891 | 33190 | - |
| sym10_262 | 12 | 28084 | 35572 | 53686 | 61183 | - |
| dc2_222 | 15 | 4131 | 5242 | 8280 | 9450 | - |
| co14_215 | 15 | 7840 | 8570 | 17074 | 19297 | - |
| mlp4_245 | 16 | 8232 | 10328 | 16572 | 18702 | - |
| hwb8_113 | 9 | 30372 | 38717 | 62619 | 79839 | - |
| qft_16 | 16 | 240 | 61 | 510 | 681 | - |
| plus63mod4096_163 | 13 | 56329 | 72246 | 115606 | 129148 | - |
| urf1_149 | 9 | 80878 | 99586 | 148531 | 166426 | - |
| urf3_155 | 10 | 185276 | 229365 | 337802 | 373985 | - |
| urf3_279 | 10 | 60380 | 70702 | 114377 | 130334 | - |
| hwb9_119 | 10 | 90955 | 116199 | 159793 | 181048 | - |
| plus63mod8192_164 | 14 | 81865 | 105142 | 165931 | 190486 | - |
| sym9_193 | 11 | 15232 | 19235 | 28378 | 31786 | - |
| ising_model_13 | 13 | 120 | 46 | 120 | 120 | - |
| urf1_278 | 9 | 26692 | 30955 | 50722 | 57343 | - |
| ising_model_16 | 16 | 150 | 57 | 150 | 150 | - |
| ground_state_estimation_10 | 13 | 154209 | 217236 | 189222 | 222867 | - |
| adr4_197 | 13 | 1498 | 1839 | 3046 | 3508 | - |
| clip_206 | 14 | 14772 | 17879 | 31062 | 35367 | - |
| cm85a_209 | 14 | 4986 | 6374 | 11250 | 11661 | - |
| rd84_253 | 12 | 5960 | 7261 | 11507 | 12959 | - |
| dist_223 | 13 | 16624 | 19694 | 33493 | 38917 | - |
| inc_237 | 16 | 4636 | 5864 | 8215 | 9637 | - |
| urf6_160 | 15 | 75180 | 93645 | 157752 | 172536 | - |

Table 10. Comparison of the depth of the output circuit on the IBM Q20